Modeling the Miocene Climatic Optimum. Part I: Land and Atmosphere*

N. HEROLD

EarthByte Group, School of Geosciences, University of Sydney, Sydney, New South Wales, Australia

M. HUBER

Earth and Atmospheric Sciences, Purdue University, West Lafayette, Indiana

R. D. MÜLLER

EarthByte Group, School of Geosciences, University of Sydney, Sydney, New South Wales, Australia

(Manuscript received 26 August 2010, in final form 9 March 2011)

ABSTRACT

This study presents results from the Community Climate System Model 3 (CCSM3) forced with early to middle Miocene (~20–14 Ma) vegetation, topography, bathymetry, and modern CO_2. A decrease in the meridional temperature gradient of 6.5°C and an increase in global mean temperature of 1.5°C are modeled in comparison with a control simulation forced with modern boundary conditions. Seasonal poleward displacements of the subtropical jet streams and storm tracks compared to the control simulation are associated with changes in Hadley circulation and significant cooling of the polar stratosphere, consistent with previously predicted effects of global warming. Energy budget calculations indicate that reduced albedo and topography were responsible for Miocene warmth in the high-latitude Northern Hemisphere while a combination of increased ocean heat transport and reduced albedo was responsible for relative warmth in the high-latitude Southern Hemisphere, compared to the present. Model–data analysis suggests Miocene climate was significantly warmer and wetter than simulated here, consistent with previous uncoupled Miocene models and supports recent reconstructions of Miocene CO_2 substantially higher than present.

1. Introduction

Relative warmth during the early to middle Miocene is well documented in marine and terrestrial records. Benthic oxygen isotope data depict a peak in deep-water temperatures at 17–14.5 Ma (Zachos et al. 2008), termed the Miocene climatic optimum, after which a significant positive isotopic shift is associated with growth of the Antarctic ice sheet and a drop in deep-water and high-latitude sea surface temperatures (SSTs). During the Miocene climatic optimum deep waters were approximately 5°–6°C warmer than present (Lear et al. 2000; Zachos et al. 2008), tropical vegetation extended poleward (Cosgrove et al. 2002; Wolfe 1985), and the East Antarctic ice sheet was smaller than present (Pekar and DeConto 2006).

Although records of Miocene warming are clear, the mechanisms responsible are not. The role of CO_2 is controversial, with Alkenone- and Boron-based proxies suggesting concentrations similar to or lower than present (Pagani et al. 1999; Pearson and Palmer 2000) and leaf stomata indicators suggesting concentrations significantly higher (Kürschner et al. 2008). Changes in ocean gateways and bathymetry have also long been proposed as catalysts for warming via modifications to ocean heat transport (Flower and Kennett 1994; Lagabrielle et al. 2009; Poore et al. 2006; Ramsay et al. 1998; Schnitker 1980; Woodruff and Savin 1989). However, analysis of some of the concomitant tectonic events (Wright and Miller 1996), the proposed mechanisms involved in gateway-induced warming (Sloan et al. 1995) and more recently coupled atmosphere–ocean modeling (Huber and Sloan 2001), show that such changes are not an easy explanation for global warmth. Nonetheless, numerous independent tectonic events occurred during the Miocene and

* Purdue Climate Change Research Center Publication Number 1113.

Corresponding author address: N. Herold, EarthByte Group, School of Geosciences, University of Sydney, Sydney, NSW 2006, Australia. E-mail: nher5224@uni.sydney.edu.au

DOI: 10.1175/2011JCLI4035.1

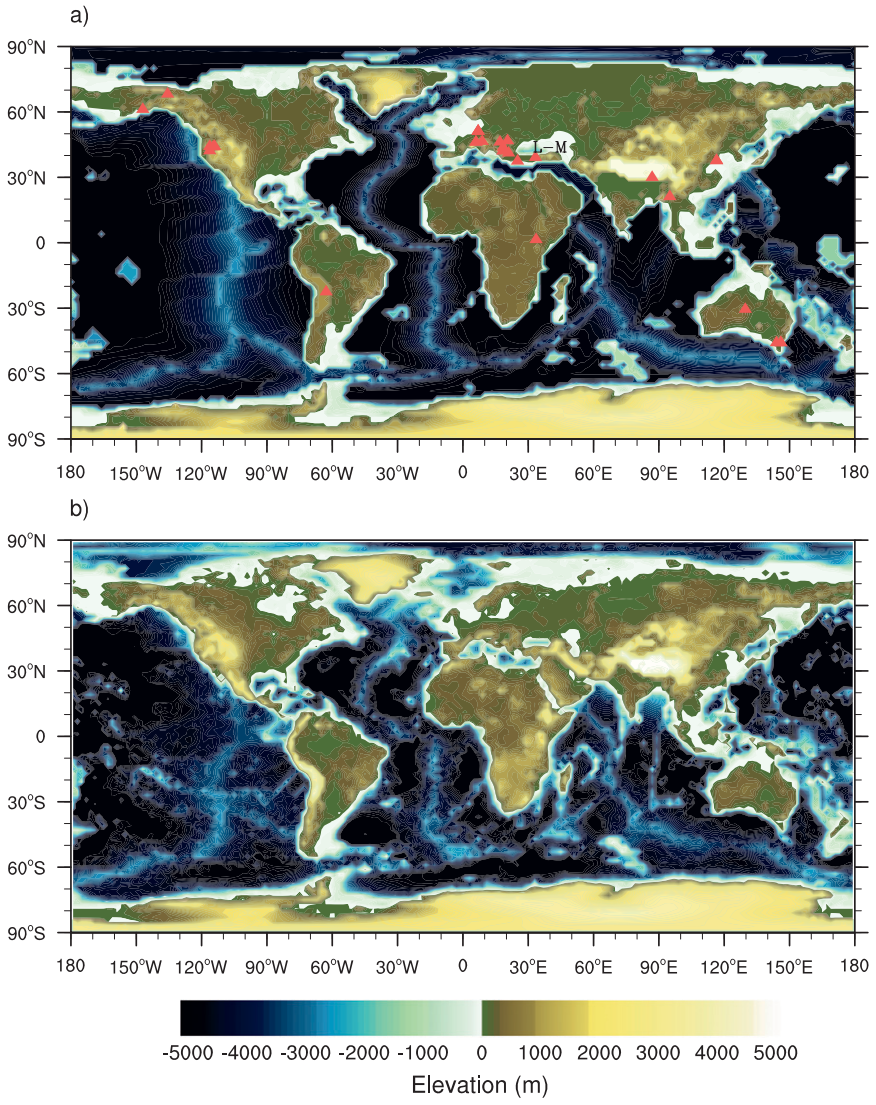

FIG. 1. Topography and bathymetry for the (a) Miocene and (b) control case. Terrestrial temperature and precipitation proxies indicated by red triangles (Tables 2 and 3). L-M indicates Lago-Mare.

the lack of a "smoking gun" for the observed climate change implies a causal and cumulative relationship (Potter and Szatmari 2009), though no hypothesis satisfactorily explains a connection. Furthermore, sparse spatial and temporal coverage of climate proxies has limited the characterization of global Miocene climate (Fig. 1a), although a renewed interest in Neogene environments has greatly improved coverage in some regions [Neogene Climate Evolution in Eurasia (NECLIME); available online at http://www.neclime.de/].

Various numerical models have been used to explore Miocene climate, including sensitivity to CO_2 (Micheels et al. 2009a; Steppuhn et al. 2007; Tong et al. 2009; You et al. 2009), SSTs (Herold et al. 2010; Lunt et al. 2008a; Steppuhn et al. 2006), vegetation (Dutton and Barron 1997; Micheels et al. 2009b; Micheels et al. 2007), bathymetry (Barron and Peterson 1991; Bice et al. 2000; Butzin et al. 2011; von der Heydt and Dijkstra 2006), or some combination of these (Fluteau et al. 1999; Henrot et al. 2010; Herold et al. 2011a; Kutzbach and Behling 2004; Langebroek et al. 2009; Micheels et al. 2011; Ruddiman et al. 1997). However, due to the relatively recent advent of coupled atmosphere–ocean models for deep time paleoclimate analysis, the majority of the above studies have relied on prescribing SSTs or ocean heat fluxes. Consequently, such studies are significantly limited by uncertainties in the paleoclimate record or by the simplifying assumptions of ocean heat transport. In a recent

study utilizing a coupled atmosphere–ocean model, von der Heydt and Dijkstra (2006) use version 1.4 of the Community Climate System Model (CCSM) to analyze the reversal of Panama throughflow between the Oligocene and early Miocene. They link this reversal to changing dimensions of Southern Ocean gateways and closing of the Tethys gateway. Using the Community Earth System Models (COSMOS), Micheels et al. (2011) take advantage of the data independence of the coupled modeling framework to analyze heat transport during the late Miocene. They find a decrease in Northern Hemisphere ocean heat transport compared to the present, likely due to the open Panama gateway in the late Miocene, and a compensating increase in atmospheric heat transport. In this study we present results from version 3 of the CCSM forced with global Miocene boundary conditions to investigate their effect on atmosphere and land climate. An important advance in our study is the representation of Miocene vegetation, topography, and bathymetry (cf. von der Heydt and Dijkstra 2006). In a companion study we focus on the ocean circulation results (Herold et al. 2011b, manuscript submitted to *Paleoceanography*). While the nonlinearity of Miocene warming (e.g., Miller et al. 1991) suggests complex feedbacks between multiple processes were involved (Holbourn et al. 2005; Shevenell et al. 2008) and uncertainty remains with respect to the causes of Miocene warmth, this study focuses on the mean background climate of the early to middle Miocene.

2. Model description

The Community Climate System Model 3 (CCSM3) consists of four component models of the atmosphere, ocean, land, and sea ice (Collins et al. 2006). Each model operates at an independent time step and communicates via a coupler. The atmosphere is represented with a hybrid sigma–pressure coordinate system resolving 26 vertical levels. The land model resolves 10 soil layers, up to five snow layers, and 16 plant functional types. Each land grid cell consists of up to four plant functional types. Both the land and atmosphere models share a horizontal T31 spectral grid, representing a resolution of 3.75° × ~3.75° in longitude and latitude, respectively. The ocean and sea ice models operate on a horizontal stretched grid of approximately 3° × ~1.5° in longitude and latitude, respectively, with coarser meridional resolution at middle latitudes and finer resolution at the equator.

The CCSM3 has been utilized extensively for present and future climate simulations (Meehl et al. 2007) as well as for simulations of the late Permian (Kiehl and Shields 2005) and Eocene epochs (Shellito et al. 2009). The low-resolution CCSM3, which corresponds closely to the resolution chosen in this study, allows for quick equilibration of multicentury simulations while maintaining a robust steady-state climate (Yeager et al. 2006). However, Yeager et al. (2006) note excessive sea ice production in both hemispheres under modern boundary conditions in this configuration of the CCSM3. Ocean heat transport is also underestimated and Southern Hemisphere storm tracks displaced equatorward compared to observations. Conversely, volume transport by the Antarctic Circumpolar Current is closer to observed values and eastern boundary current SST biases are least severe in the low-resolution CCSM3, compared with higher-resolution configurations (Yeager et al. 2006).

3. Experiment design

Our Miocene case is configured with topography and bathymetry from Herold et al. (2008), with minor adjustments to sea level and the Tethys gateway (cf. Fig. 1a). Dating of Tethys gateway closure(s) is controversial with most evidence suggesting terminal closure by the middle Miocene (Ramsay et al. 1998; Rögl 1999). As some researchers have attributed early to middle Miocene warmth to Tethyan outflow of relatively warm, saline deep water (Flower and Kennett 1995; Ramsay et al. 1998; Woodruff and Savin 1989), we choose an open configuration to enable such outflow to occur. Major topographic differences between the Miocene and modern day are accounted for by paleoelevation estimates and include areas such as the Tibetan Plateau and Andean Cordillera (see Herold et al. 2008 for details). Plant functional types are prescribed based on Herold et al. (2010).

Concentrations of CO_2 during the Miocene are controversial. In this study we prescribe a concentration of 355 ppmv, midway between the majority of Miocene estimates and the same as used in 1990 control CCSM3 experiments. N_2O and CH_4 are set to preindustrial concentrations of 270 and 760 ppb, respectively. Aerosol radiative forcing is significantly reduced from the modern. The solar constant is set to 1365 W m^{-2} (compared to 1367 W m^{-2} for control CCSM3 simulations), and obliquity, eccentricity, and precession are set to values appropriate for 1950.

Initial ocean temperatures and salinities are based on modern global depth averages. This arbitrary initialization results in an ocean equilibration time of approximately 800 years, which is evaluated based on depth-integrated ocean mean temperature. We integrate the model for a further 300 years and use the mean of the last 100 years for analysis. Residual energy flux at the surface and top of the model for the final 100 years is 0.1 W m^{-2} and volume mean ocean temperature drift is

TABLE 1. Global mean CCSM3 diagnostics.

	Miocene	Control
Residual top of model energy flux (W m^{-2})	−0.086	0.023
Residual surface energy flux (W m^{-2})	−0.109	0.003
Surface temperature (°C)	15.38	13.88
Surface temperature–land only (°C)	8.70	7.41
Surface albedo	0.11	0.15
Cumulative precipitation (mm yr^{-1})	104	99
Net shortwave radiation at surface (W m^{-2})	163.5	158.6
Net longwave radiation at surface (W m^{-2})	57.9	57.8
Sensible heat flux (W m^{-2})	22.6	21.6
Latent heat flux (W m^{-2})	83.1	79.2

<0.01°C $century^{-1}$ (Table 1). We compare our Miocene case with a control case forced with modern boundary conditions appropriate for 1990, including a CO_2 concentration of 355 ppmv.

4. Results

a. Surface temperature

Global annual surface temperature is 1.5°C higher in the Miocene compared to the control case (Table 1). Zonal mean tropical temperatures in the Miocene are 0.5°C lower while polar temperatures are approximately 6°C higher, resulting in a 6.5°C lowering of the meridional temperature gradient (Fig. 2a). Maximum warming at both poles in the Miocene relative to the control case is approximately equal; however, the majority of polar warming in the Northern Hemisphere manifests over land, in contrast to the meager temperature increase over Antarctica (Fig. 2b). At low to middle latitudes, patterns of mean annual surface temperature do not vary considerably between the Miocene and control cases, with most isotherms shifted poleward by several degrees in the Miocene (Figs. 3c and 3f). Parts of Australia are more than 3°C cooler in the Miocene as it lay outside of the tropics. Reduced Miocene topography in Greenland and North America contributes to higher annual temperatures in these regions. Summertime temperatures in Greenland and a large portion of the Arctic Ocean are above freezing in the Miocene, in contrast to the control case (Figs. 3a and 3d). A significant portion of the modeled surface warming, particularly at high latitudes, can be attributed to the prescribed darker- and broader-leaved Miocene vegetation compared to the control case (Herold et al. 2010). Dutton and Barron (1997) showed that differences in vegetation between the present and Miocene contribute a 1.9°C global warming effect. Similarly, Otto-Bliesner and Upchurch (1997) showed that a vegetated versus unvegetated Cretaceous world results in a 2.2°C global warming. More recent studies with less idealized vegetation distributions show the same sign of sensitivity to

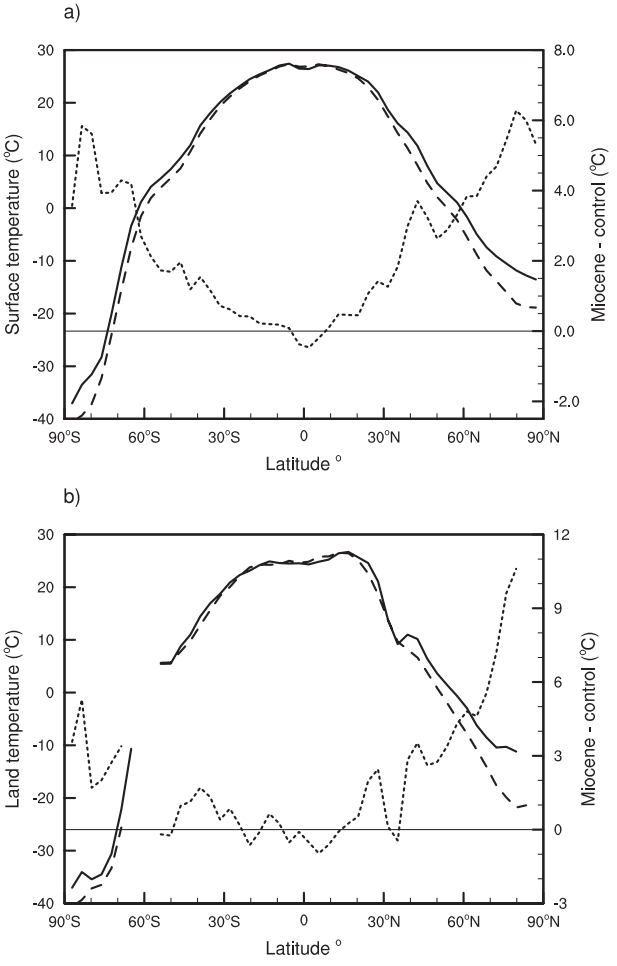

FIG. 2. Zonal mean (a) surface temperature and (b) land temperature for the Miocene (solid) and control case (dashed). Dotted line indicates anomaly (right *y* axis).

vegetation, though of a significantly smaller magnitude. Micheels et al. (2007) report a climate sensitivity to late Miocene vegetation of 0.9°C, while Henrot et al. (2010) report a 0.5°C sensitivity to middle Miocene vegetation, relative to modern vegetation. Given that total global warming in our Miocene case is 1.5°C relative to the control case, in lieu of a sensitivity experiment we speculate that the warming from our Miocene vegetation alone is closer to these latter studies. Significant increases in continental seasonality occur in the Miocene Northern Hemisphere due namely to the greater surface area of Eurasia and North America (Figs. 3d and 3e).

b. Atmospheric temperature

Miocene temperatures in the polar troposphere and stratosphere (above 200 mb) are warmer and cooler than the control case, respectively, particularly in the Northern Hemisphere, resulting in a larger vertical temperature

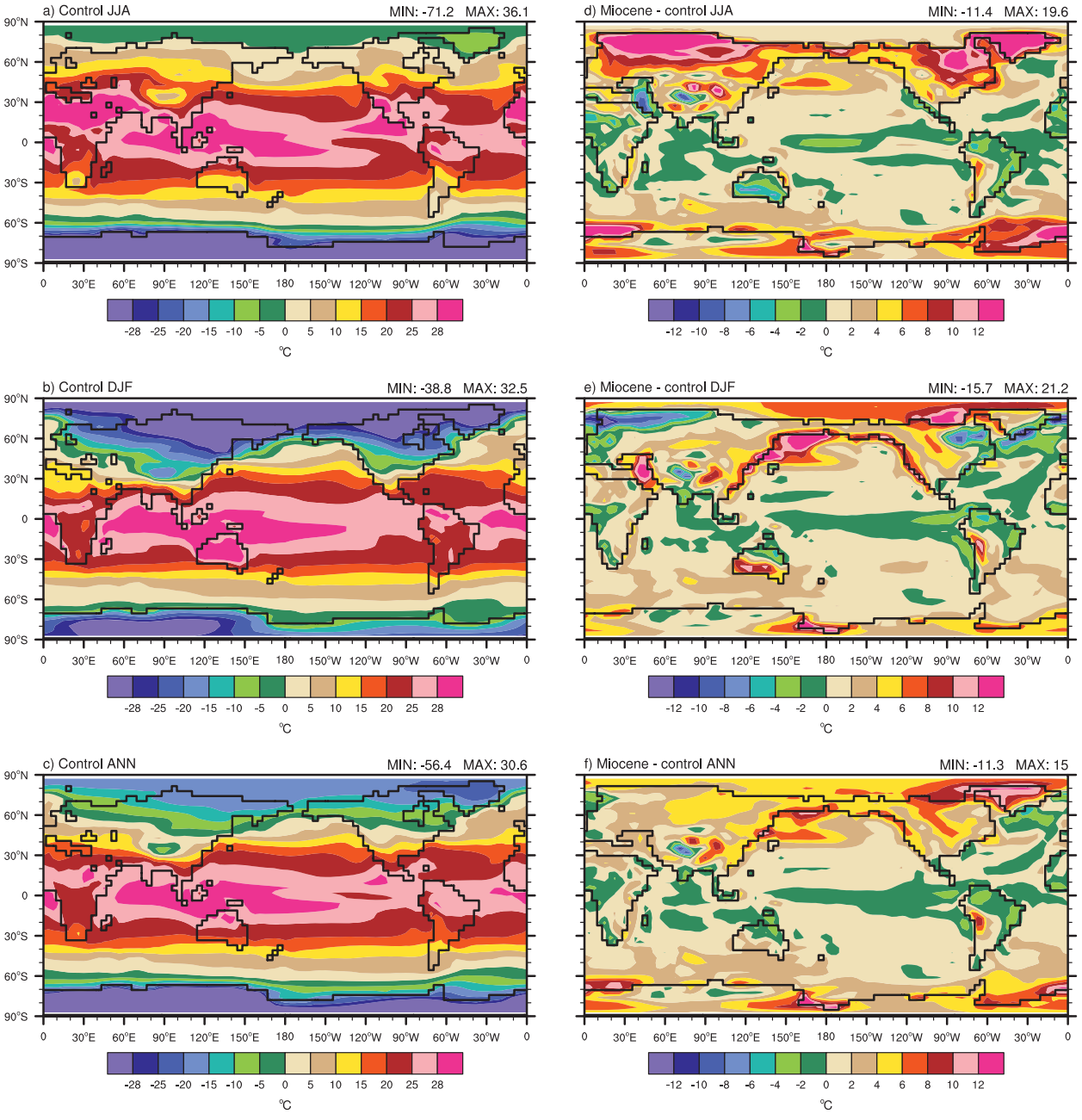

FIG. 3. Control case surface temperatures for (a) June–August, (b) December–February, and the (c) annual mean. (d)–(f) Miocene − control case surface temperature anomalies.

gradient (Figs. 4c and 4d). Cooling of the northern polar stratosphere during wintertime increases relative humidity and consequently increases high-altitude cloud fraction by up to 20% (not shown). However, a corresponding Southern Hemisphere wintertime cooling is not observed (Fig. 4c). Substantially greater summertime warming occurs in the northern polar troposphere compared to the southern polar troposphere in the Miocene (cf. Figs. 4c and 4d). This is associated with the large increase in surface area of northwest Eurasia as well as reduced surface albedo across northeast North America and Greenland. Comparatively little albedo change—and thus temperature change—is modeled over the Antarctic continent during the Southern Hemisphere summer. Interestingly, the majority of warming that occurs in the southern polar troposphere occurs concomitantly with warming in the northern polar troposphere, though to a lesser degree (Fig. 4c). This is attributed to the greatest decrease in

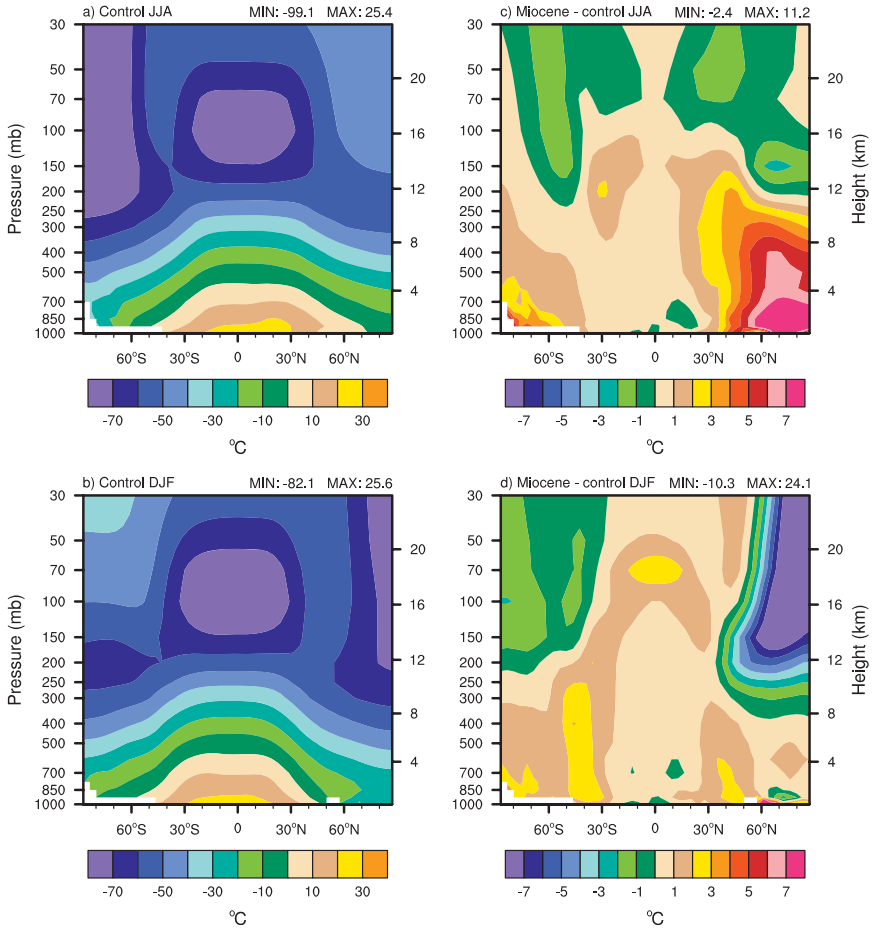

FIG. 4. Zonal atmospheric temperature for the control case during (a) June–August and (b) December–February (b). (c),(d) Miocene − control case anomalies.

Southern Ocean sea ice occurring during Southern Hemisphere wintertime, driven by significant Weddell Sea bottom water formation (Herold et al. 2011b, manuscript submitted to *Paleoceanography*).

c. Jet streams and storm tracks

The subtropical jet streams in the Miocene are weaker than our control case (Fig. 5); an expected result given the lower meridional temperature gradient (Fig. 2a). The subtropical jet streams are displaced poleward and slightly upward during December–February (DJF), though not during June–August (JJA; Figs. 5c and 5d). Similarly, intensification of the Miocene northern polar jet stream occurs during DJF, though no corresponding intensification of the Southern Hemisphere polar jet stream is observed during JJA, mirroring simulated stratospheric temperature changes (previous section). Consistent with zonal circulation changes, the zonal distribution of eddy kinetic energy indicates a poleward displacement of middle-latitude storms during DJF in both hemispheres, though only a weakening of storm tracks during JJA (Fig. 6). The poleward displacement of eddy kinetic energy is also consistent with a poleward shift in Hadley circulation (Fig. 7).

d. Seasonal precipitation and surface winds

The Miocene case exhibits broad increases in mean annual precipitation over central and northern Africa, northern Eurasia, North America (>50°N), and Greenland, the majority of which falls during JJA (Figs. 8a and 8d). Because of the variation in plate configurations between the Miocene and present day, anomaly plots between the two cases are ineffective at examining the regional monsoons. Therefore we examine DJF minus JJA surface wind and precipitation fields for each case, which enables a qualitative assessment of monsoon strength and seasonal drying–wetting (Figs. 8 and 9). In the Miocene case smaller seasonal variations in wind strength relative to the control case are modeled over India, the Arabian Sea, the South China Sea, and along the coast of the northwest Pacific Ocean (Figs. 9c and 9f). These

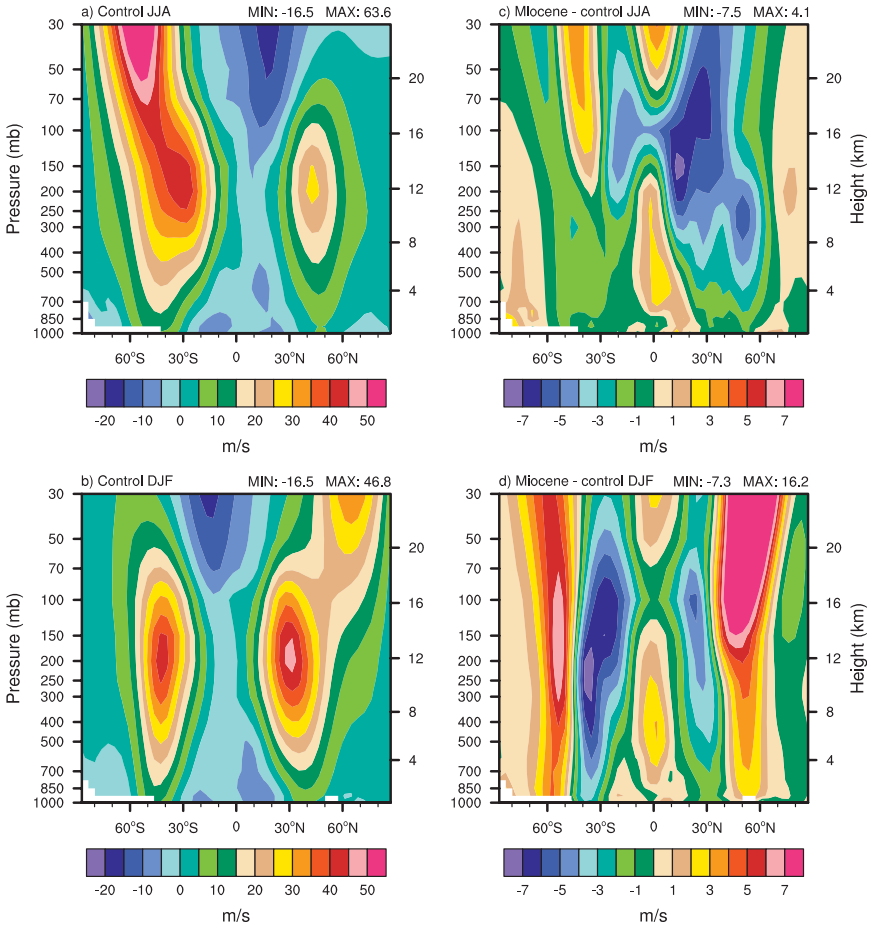

FIG. 5. As in Fig. 4, but for zonal wind.

differences reflect a weakening of JJA onshore winds from the Arabian Sea and weakening of DJF offshore winds in the northwest Pacific Ocean in the Miocene. In contrast, stronger JJA onshore winds over the Bay of Bengal occur in the Miocene case. These changes are accompanied by greater maxima in seasonal precipitation change over southern and eastern Eurasia in the Miocene relative to the control case (Figs. 8c and 8f). In each instance this is due overwhelmingly to higher JJA precipitation in the Miocene case than to differences in DJF precipitation (Figs. 8a and 8d). More northward landfall of summer precipitation into northeast China in the Miocene case (Figs. 8a and 8d) is consistent with luvisols indicating greater northward moisture transport compared to the Quaternary (Guo et al. 2008). Generally, however, the changes in Asian monsoon strength between our Miocene and control cases are not strong relative to the simulated effects of Tibetan Plateau uplift or Paratethys expansion (Zhongshi et al. 2007b). As the Tibetan Plateau has a near-modern elevation in our Miocene case, such effects are minimal (Fig. 1).

The present-day asymmetry in seasonality about the Rocky Mountains is amplified in the Miocene case, with wetter winters to the northwest and wetter summers to the southeast (Figs. 8c and 8f). This is in contrast to paleobotanical evidence suggesting wet summers in the western United States (Lyle et al. 2008). Summertime onshore winds over northern Australia are substantially weaker in the Miocene case and thus summer monsoon precipitation is significantly weaker over the northern half of the continent. We do not relate this to reduced atmospheric outflow from the Asian winter monsoon (see Miller et al. 2005) but to the location of Australia within the subtropical high in the Miocene. Relatively modest sensitivities to changes in local and global boundary conditions demonstrate the robustness of a weaker Australian monsoon in our model (Herold et al. 2011a). In northern Africa, summer precipitation is significantly higher in the Miocene because of the replacement of desert with broadleaf vegetation (Figs. 8a and 8d), consistent with the sensitivity study of Micheels et al. (2009b).

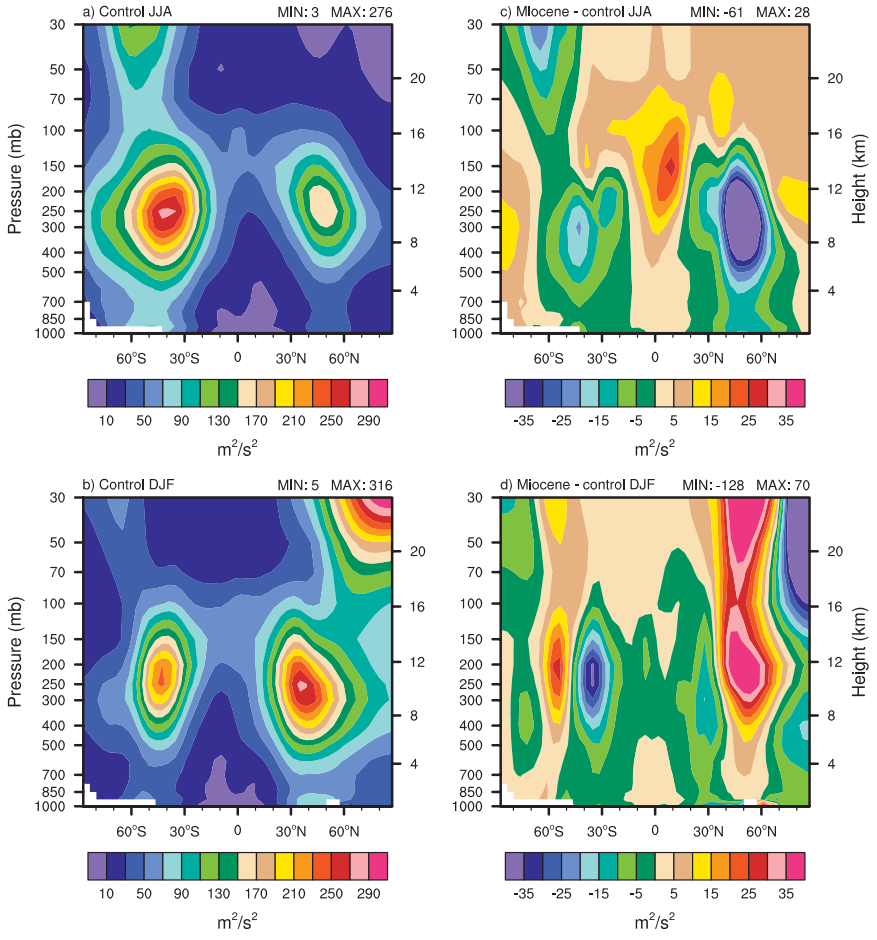

FIG. 6. As in Fig. 4, but for eddy kinetic energy.

e. *Energy budget*

Atmospheric heat transport differs little between the Miocene and control cases with the largest difference being a weaker peak at 45°N in the Miocene by 0.5 PW (Fig. 10). Similarly, ocean heat transport decreases in the Northern Hemisphere by approximately the same magnitude, thus changes in atmospheric heat transport do not compensate for changes in ocean heat transport (or vice versa) as modeled by Micheels et al. (2011). Decreased Northern Hemisphere ocean heat transport in the Miocene case is a result of a significant weakening of North Atlantic Deep Water formation (Herold et al. 2011b, manuscript submitted to *Paleoceanography*). A slight poleward shift in peak atmospheric heat transport is associated with a poleward shift in peak eddy kinetic energy (Fig. 6). A near-zero residual surface energy flux at latitudes greater than 60°N indicates radiative equilibrium is achieved without a compensating ocean heat transport (Fig. 11). This increase in residual surface energy compared to the control case is due primarily to greater incoming net surface energy over the sub-Arctic continents in association with vegetation and topography changes. Southern Hemisphere heat transport by the atmosphere decreases slightly, though it is over compensated by an increase in ocean heat transport.

f. *Quantitative comparison with climate proxies*

While proxy records are inconsistently distributed (Fig. 1a) and often subject to large uncertainties (as discussed by Herold et al. 2010), they provide the only means of ground truth for our Miocene case. Comparisons between models and proxies also introduce their own bias due to inherent model uncertainties. The CCSM3 is capable of stable multi-millennial climate simulations and is significantly improved over earlier versions. However, it contains significant systematic biases in modeling the present climate (Collins et al. 2006). For example, the high-resolution CCSM3 simulates mean summer 2-m air temperatures up to ±16°C different from observations (Collins et al. 2006). Somewhat surprisingly, the same discrepancy is smaller for our low-resolution control case, though of

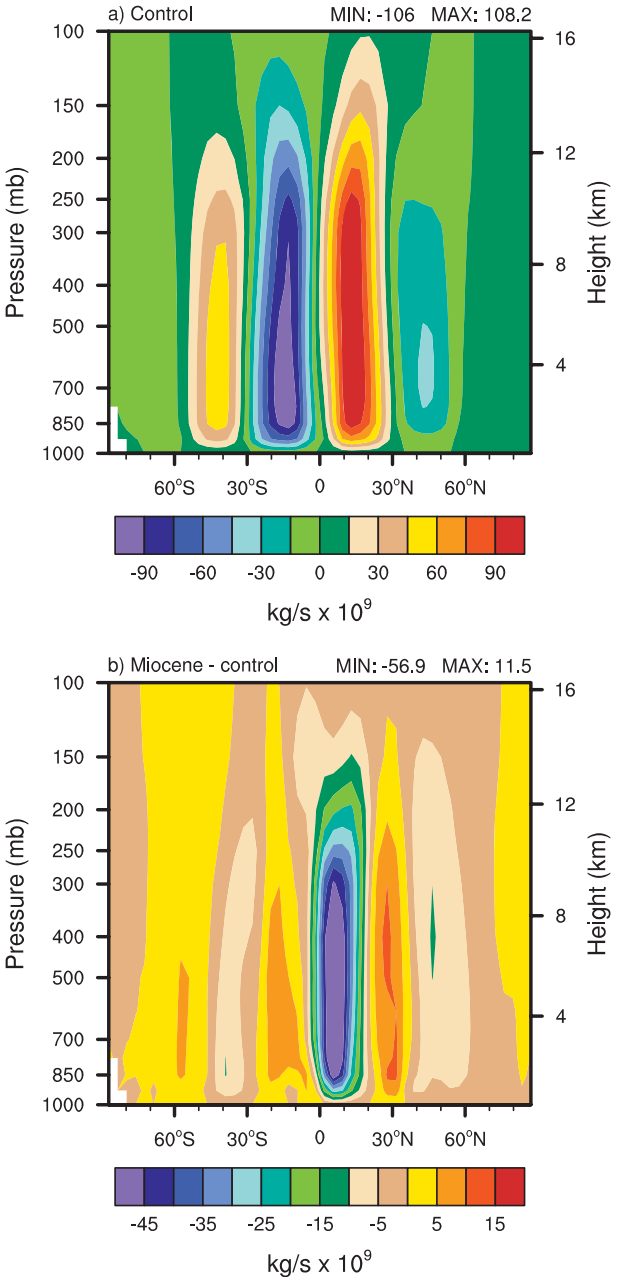

FIG. 7. Annual meridional overturning circulation for the (a) control case and the (b) Miocene − control case anomaly.

a similar magnitude. Thus we compare the differences in 2-m air temperature and precipitation between our Miocene and control cases to the differences between Miocene proxy records and modern observations (Tables 2 and 3). Here, 2-m air temperature is chosen as it is a closer representation of the forest canopy, from which most terrestrial proxies of climate are derived. Examination of Table 2 clearly shows that simulated changes in temperature at proxy localities (the simulated warming column) are significantly lower than the changes based on modern observations and proxy records (the proxy-derived warming column). The mean warming across all proxy locations between our Miocene and control cases is 1.3°C, compared to 5.9°C between observations and proxies (Table 2). Thus our Miocene case is significantly too cool. The largest differences between simulated and observed Miocene warmings occur at middle- to high-latitude localities, indicating that the meridional temperature gradient is significantly steeper than indicated by proxies, consistent with previous Miocene climate modeling (Steppuhn et al. 2007; Tong et al. 2009).

We note that there is a clear distribution bias toward the Tethys Sea (Fig. 1a), thus model–data discrepancies are not necessarily indicative of global model performance. However, the mean simulated warming among proxy sites (1.3°C; Table 2) is similar to the mean global warming between the Miocene and control cases (1.5°C; Table 1). Precipitation change follows a similar trend to 2-m air temperature, with differences between observations and proxies significantly higher than the differences between our Miocene and control cases (Table 3).

5. Discussion

a. Miocene warmth

Our Miocene case exhibits a decrease in the meridional temperature gradient of 6.5°C and an increase in global mean temperature of 1.5°C compared with our control case, without a higher CO_2. This warming is equivalent to the transient climate response of the CCSM3 to a doubling of CO_2 (Kiehl et al. 2006) and suggests that differences in topography, bathymetry, and vegetation contributed significantly to Miocene warmth. However, the middle-latitude divergence of modeled temperature change from observed temperature change indicates that the Miocene case's meridional temperature gradient is too steep (Table 2) and that global mean temperature was higher than simulated here. This is consistent with previous Miocene studies using slab (Micheels et al. 2007; Steppuhn et al. 2007; Tong et al. 2009; You et al. 2009) and dynamical ocean models (Micheels et al. 2011).

High-latitude warming in our Miocene case is compensated to a large extent by meager increases and even decreases in tropical temperatures (Fig. 3f). This is in stark contrast to the late Miocene coupled atmosphere–ocean simulation by Micheels et al. (2011), which exhibits zonal mean tropical temperatures over 1°C warmer than modern (their Fig. 3a). A large portion of this difference can be attributed to increased upwelling of cool waters in the tropical Pacific in our Miocene case, ostensibly as a response to the open Panama gateway. A similar surface temperature response to opening of the Panama gateway

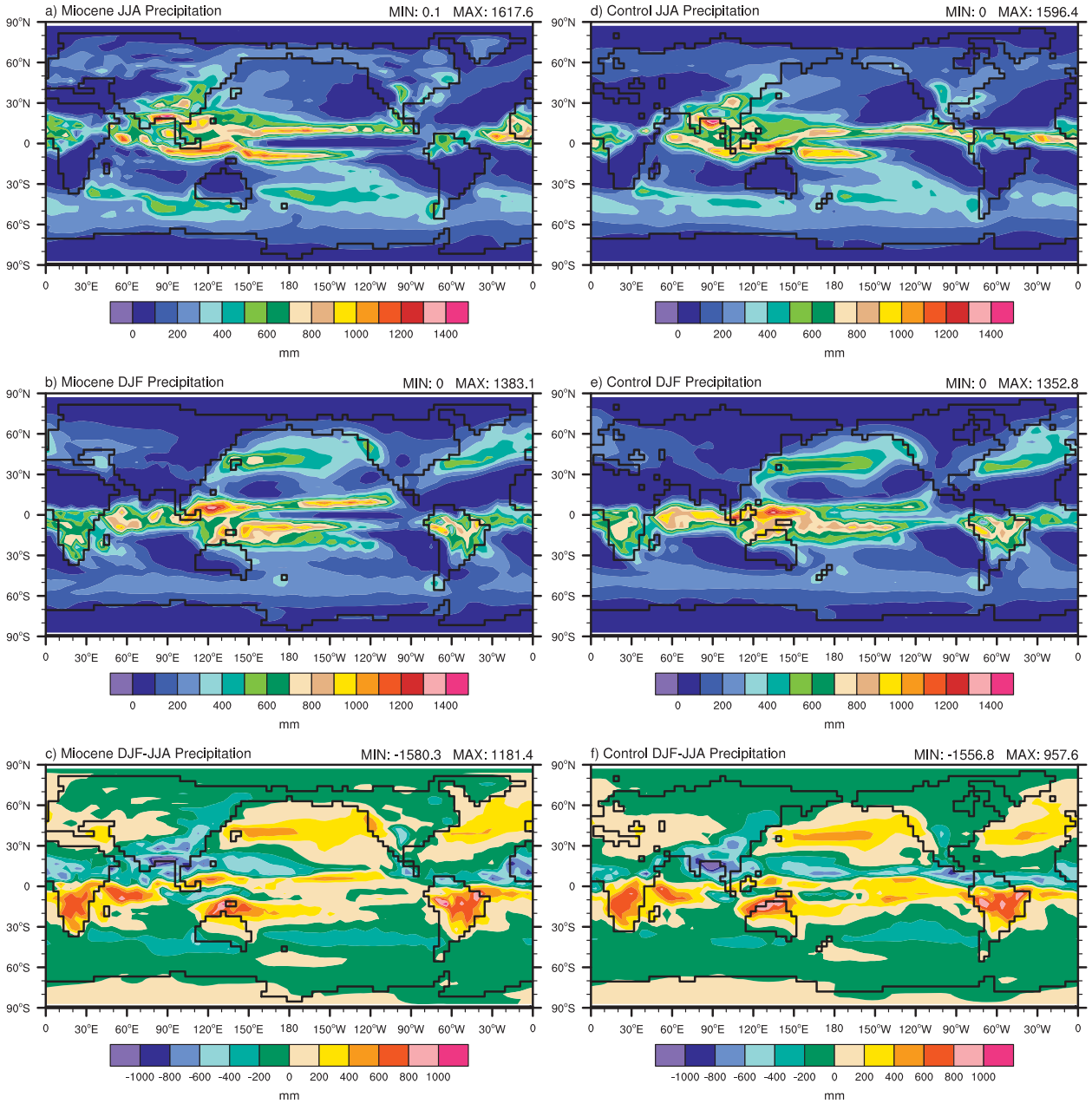

FIG. 8. Precipitation for the (a)–(c) Miocene and (d)–(f) control case for JJA, DJF, and DJF − JJA anomalies.

is simulated by Lunt et al. (2008c). The reconciliation of simulated tropical temperatures with proxy records is precluded by the absence or poor fidelity of data.

Northern Hemisphere polar stratospheric cooling in the Miocene case occurs almost entirely during polar night, decreasing minimum temperatures to approximately −88.8°C (Fig. 4d). This is several degrees below the formation threshold of stratospheric clouds (~−83.2°C), suggesting these may have been a viable mechanism for high-latitude warming (e.g., Sloan and Pollard 1998). We note that the region of stratospheric temperatures below the formation threshold in our Miocene case is small (>80°N) and that lower temperatures would likely be required before stratospheric clouds could have a significant surface effect (Rosenfield 1993). However, higher concentrations of stratospheric CH_4 (Beerling et al. 2009) and a warmer tropical tropopause (Randel et al. 2006) due to higher CO_2 (e.g., Kürschner et al. 2008) may have further promoted conditions conducive to stratospheric cloud formation.

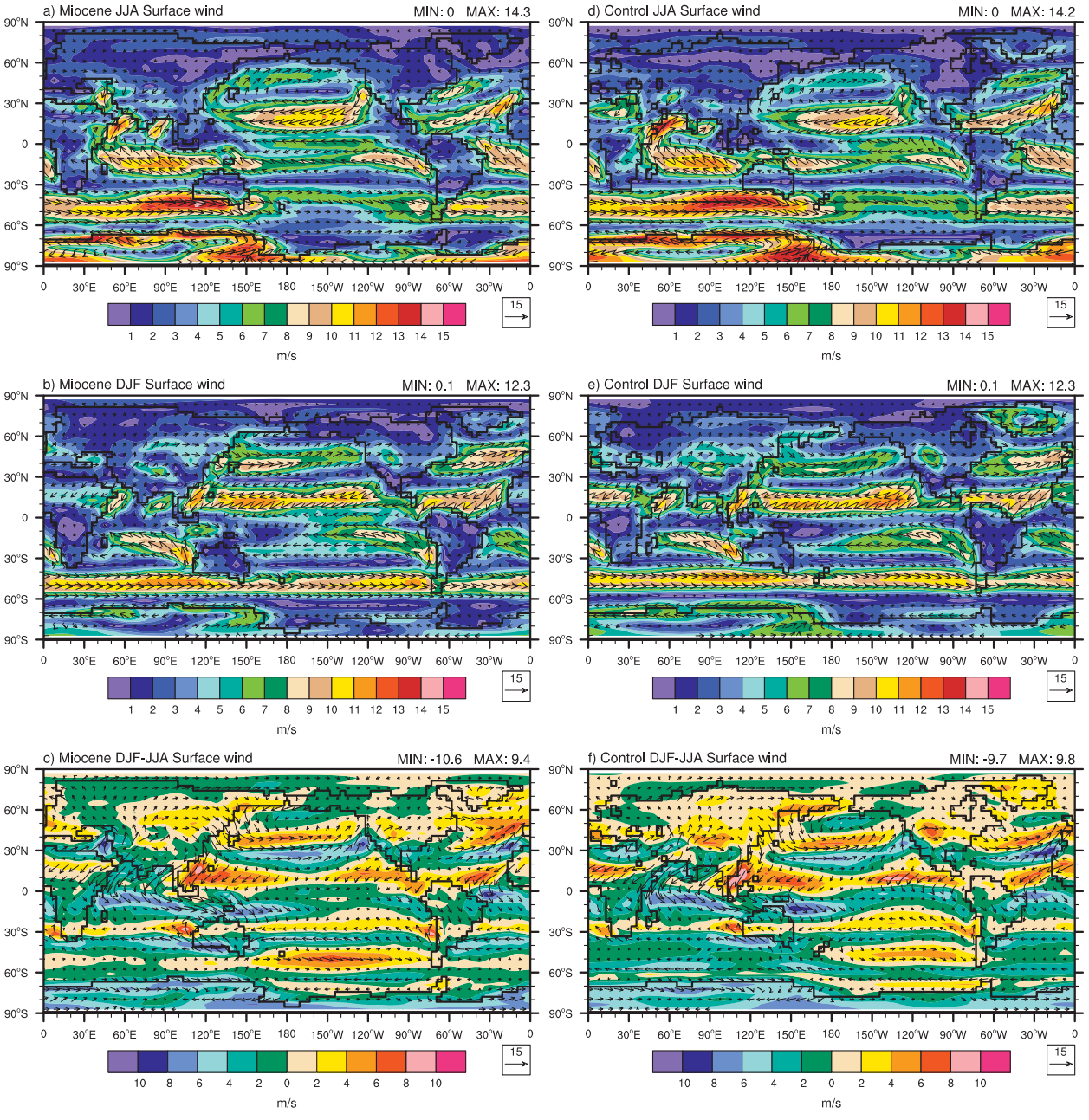

FIG. 9. As in Fig. 8, but for surface wind.

Because of sparse and ambiguous proxy records, the timing of Northern Hemisphere glaciation has been the subject of debate. Sediment records from the central Arctic basin indicate the existence of sea ice from ~45 Ma (Moran et al. 2006) and ice-rafted debris indicate isolated glaciers in Greenland between 30–38 Ma (Eldrett et al. 2007), much earlier than previous records suggested (e.g., Larsen 1994; Zachos et al. 2001). However, the onset of major permanent ice sheets in Greenland likely did not occur until CO_2 dropped below preindustrial concentrations (DeConto et al. 2008; Lunt et al. 2008b). This latter supposition is supported here by simulated above-freezing summertime temperatures over Greenland in our Miocene case (Figs. 3a and 3d), despite a modern CO_2 and an overproduction of sea ice (Herold et al. 2011b, manuscript submitted to *Paleoceanography*). This surface warming compared to our control case is attributable to the lower elevation and prescribed needleleaf vegetation of Greenland in the Miocene case.

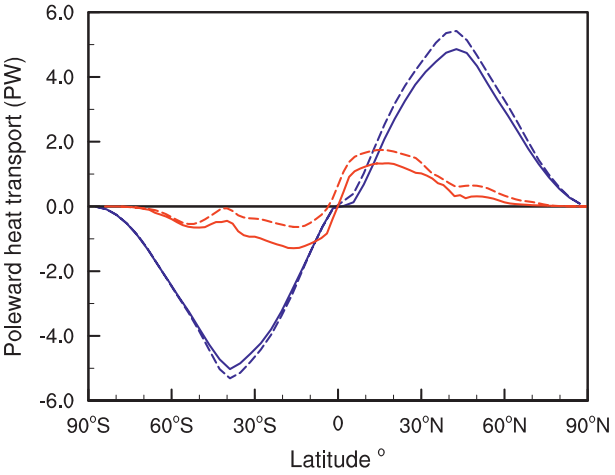

FIG. 10. Ocean (red) and atmosphere (blue) heat transport for the Miocene (solid) and control case (dashed).

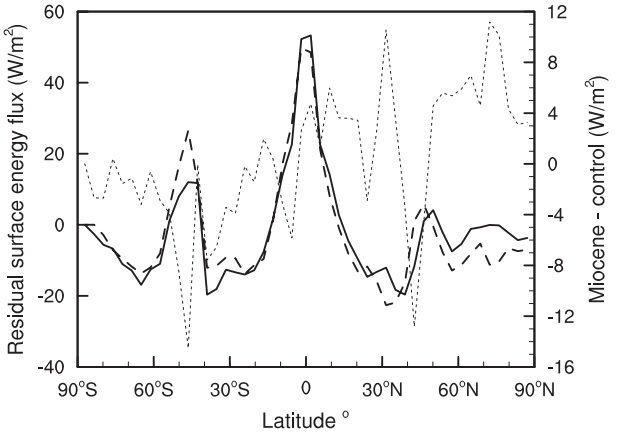

FIG. 11. Residual surface energy flux for the Miocene (solid line) and control case (dashed line). Dotted line indicates anomaly (right axis).

Miocene heat transport by the atmosphere is lower in the Northern Hemisphere and consequently does not contribute to the higher surface temperatures relative to the control case (Fig. 10). The near-zero residual surface energy flux at latitudes greater than 60°N (Fig. 11) indicates that the net effect of ocean heat transport is also negligible in the Miocene, as shown by a more than halving of ocean heat transport past this latitude (Fig. 10). Consequently, changes in albedo and topography are responsible for high-latitude Northern Hemisphere warming. This is consistent with models of early (Heinemann et al. 2009) and late (Haywood and Valdes 2004) Cenozoic climates as well as various sensitivity studies (Dutton and Barron 1997; Otto-Bliesner and Upchurch 1997). Conversely, Miocene high southern latitudes show near-identical atmospheric heat transport compared to the control case though a slightly lower residual surface energy flux (Fig. 11) and greater ocean heat transport (Fig. 10; Herold et al. 2011b, manuscript submitted to *Paleoceanography*), resulting in significantly higher surface temperatures over the ocean (cf. Figs. 2a and 2b). This high-latitude warming occurs predominantly at the site of Weddell Sea bottom water formation and to a lesser extent at gird points converted from land in the control case to ocean in the Miocene case (Fig. 3f). Thus the majority of high-latitude Southern Hemisphere warming is due to heat transport to the Weddell Sea and albedo changes associated with a smaller Antarctic continent.

b. Seasonal hydrology

Recent sensitivity studies have demonstrated that in addition to Tibetan Plateau uplift (Prell and Kutzbach 1992), shrinking of the Lago-Mare (Zhongshi et al. 2007b) and expansion of the South China Sea (Zhongshi et al. 2007a) were critical to the development of a monsoon climate in Asia. Our results support the transition to a modern monsoon climate by the early Miocene, as indicated by an exhaustive analysis of proxy records from the Paleocene to present (Guo et al. 2008). While uncertainty exists regarding the area and elevation of the Miocene Tibetan Plateau (Harris 2006 and references therein; Wang et al. 2008), the precipitation patterns shown here would likely be robust under a wide range of imposed elevations (Prell and Kutzbach 1992; Zhongshi et al. 2007b). Furthermore, model simulations have demonstrated that the size of the Lago-Mare has little impact on the development of the East Asian monsoon once the elevation of the Tibetan Plateau reaches approximately 3000 m and thus is not a large source of uncertainty in our study (Zhongshi et al. 2007a,b). Expectedly then, the existence and dimensions of the Asian monsoon in our Miocene case has been largely predetermined by the near-modern elevation of the Tibetan Plateau.

The northwest coast of the United States experiences higher wintertime precipitation in the Miocene case, though no change in summertime precipitation (Fig. 8). Additionally, no change in summertime effective moisture (evaporation minus precipitation) is observed (not shown). This reflects an amplification of modern-day seasonality when conversely fossil flora indicates wet summers along the west coast during the Miocene (Lyle et al. 2008). It has been suggested that wetter summers in the western United States may have been driven by warmer North Pacific SSTs (Lyle et al. 2003). The warmer SSTs in our Miocene case suggest that this was not the case. Unpublished results from an identical Miocene simulation run with a CO_2 concentration of 560 ppmv shows greater annual precipitation along the west coast of Canada but no significant change in the western United States.

TABLE 2. Temperature change simulated by the CCSM3 vs change between modern observations and proxy records. Note that proxy records are from Herold et al. (2010).

Location	Paleo lon/lat[a]	Control case 2-m air temp (°C)	Miocene case 2-m air temp (°C)	Simulated warming (°C)[b]	Modern observed 2-m air temp (°C)[c]	Miocene proxy temp (°C)[d]	Proxy-derived warming (°C)[e]	References[f]
Weisselster and Lausitz Basin, NE Germany	7/52	5.5	7.3	1.8	8.6	18	9.4	1
Lower Rhine Embayment, NW Germany	7/52	5.5	7.3	1.8	8.6	18.25	9.7	2
Schrotzberg, Southern Germany	6/47	8.8	7.4	−1.4	8.5	15.5	7.0	3
NW Bulgaria	21/42	11.5	13.6	2.1	6.8	17	10.2	4
Lower Rhine Embayment, NW Germany	7/52	5.5	7.3	1.8	8.6	15.95	7.4	5
Schrotzberg, Southern Germany	6/47	8.8	7.4	−1.4	8.5	15.45	7.0	6
Kovago-old al	17/47	8.1	9.0	0.9	10.4	18.65	8.2	7
Southern Germany (see ref for locations)	8.9/47.3	8.2	7.4	−0.8	8.0	18.95	10.9	8
Ukraine	20.5/47.6	8.1	9.0	0.9	10.0	17	7.0	9
Bigadic, Turkey	25.1/38.3	14.9	16.7	1.8	12.9	19.25	6.3	10
Samsun–Havza, Turkey	33.3/40	11.8	14.6	2.8	8.5	19	10.5	10
Pannonian Basin	18.5/44.55	7.8	11.8	4.0	10.4	15.25	4.8	11
Popovac, Serbia	18.3/42.9	11.5	11.8	0.3	8.9	17.85	8.9	12
Latrobe Valley, SE Australia	146/−45	12.8	11.0	−1.8	14.2	19	4.8	13
Bacchus Marsh, SE Australia	144/−45	15.7	10.8	−4.9	13.0	13	0.0	14
Yallourn, SE Australia	146/−45	12.8	11.0	−1.8	14.2	15.5	1.3	15
Kangaroo Well, Central Australia	129.7/-29.7	23.9	20.7	−3.2	21.2	17	−4.2	16
Yunnan Province, SW China	95/22	23.0	23.7	0.7	23.1	19.65	−3.5	17
Shanwang, China	116.5/38.5	8.4	10.1	1.7	12.8	16.25	3.4	18
Shanwang, China	116.5/38.5	8.4	10.1	1.7	12.8	12.7	−0.1	19
Shanwang, China	116.5/38.5	8.4	10.1	1.7	12.8	10.35	−2.5	20
Namling Basin, Southern Tibet	86.9/30.8	−5.1	−1.8	3.3	−2.3	6.8	9.1	21
Picture Gorge Subgroup, North America	−114.7/44.8	3.4	6.8	3.4	7.1	12	4.9	22
Eastern Oregon, North America	−114/45	3.4	5.3	2.0	7.1	12.7	5.6	23
Alaska, North America	−135.6/69	−11.3	−6.8	4.4	−7.7	9	16.7	24
Cape Blanco, North America	−116.3/45	9.1	7.4	−1.7	7.1	16.6	9.5	25
Waeaverville, North America	−116.3/43	6.1	9.3	3.2	7.3	16.2	8.9	25
Cook Inlet, North America	−147/62	−6.7	−0.1	6.6	2.4	11.2	8.8	26
Potosi, Bolivia	−62.8/−21.7	16.8	24.9	8.1	12.3	21.6	9.3	27
Fejej, Ethiopia	33.6/2.3	23.0	24.3	1.3	28.9	26	−2.9	28
			Mean:	1.3			5.9	

[a] Where paleocoordinates are not provided by reference values are calculated using modern coordinates, a plate kinematic model, and the rotations of Müller et al. (2008).

[b] Column three subtracted from column four.

[c] Uses the dataset of Willmott and Matsuura (2001) for 2-m air temperature spanning 1950–99.

[d] Where a range of values is given, the midpoint is used.

[e] Column six subtracted from column seven.

[f] References used in the table and their assigned number in the column are as follows: 1) Mosbrugger et al. (2005); 2) Utescher et al. (2000); 3) Uhl et al. (2006); 4) Ivanov et al. (2002); 5) Mosbrugger and Utescher (1997); 6) Uhl et al. (2003); 7) Uhl et al. (2007); 8) Bohme et al. (2007); 9) Syabryaj et al. (2007); 10) Akgün et al. (2007); 11) Erdei et al. (2007); 12) Utescher et al. (2007); 13) Sluiter et al. (1995); 14) Greenwood (1994); 15) Kemp (1978); 16) Megirian et al. (2004); 17) Zhao et al. (2004); 18) Liang et al. (2003); 19) Yang et al. (2007); 20) Sun et al. (2002); 21) Spicer et al. (2003); 22) Sheldon (2006); 23) Retallack (2004); 24) White and Ager (1994); 25) Wolfe (1994a); 26) Wolfe (1994b); 27) Gregory-Wodzicki et al. (1998); and 28) Wiemann et al. (1999).

TABLE 3. Precipitation change simulated by the CCSM3 vs change between modern observations and proxy records. Note that proxy records are from Herold et al. (2010).

Location	Paleo lon/lat[a]	Control case precipitation (mm)	Miocene case precipitation (mm)	Simulated precipitation change (mm)[b]	Modern observed precipitation (mm)[c]	Miocene proxy precipitation (mm)[d]	Proxy derived precipitation change (mm)[e]	References[f]
Weisselster and Lausitz Basin, NE Germany	7/52	771.8	942.9	171.1	685.7	1300	614.3	1
Lower Rhine Embayment, NW Germany	7/52	771.8	942.9	171.1	685.7	1350	664.3	2
Schrotzberg, Southern Germany	6/47	813.7	1154.1	340.4	1109	1300	191	3
NW Bulgaria	21/42	504.7	568.1	63.4	693.7	1200	506.3	4
Lower Rhine Embayment, NW Germany	7/52	771.8	942.9	171.1	685.7	1293	607.3	5
Southern Germany (see ref for locations)	8.9/47.3	807.1	1154.1	347.0	1222.4	1146	−76.9	8
Ukraine	20.5/47.6	609.0	941.5	332.6	588.5	1168	579	9
Bigadic, Turkey	25.1/38.3	391.4	436.7	45.3	758.7	1270	510.8	10
Samsun–Havza, Turkey	33.3/40	374.6	648.7	274.1	413	1270	856.5	10
Pannonian Basin	18.5/44.6	714.1	664.9	−49.2	550.2	1074	523.8	11
Popovac, Serbia	18.3/42.9	504.7	664.9	160.2	789.3	1434	644.7	12
Latrobe Valley, SE Australia	146/−45	375.0	798.1	423.1	832.2	1700	867.8	13
Yallourn, SE Australia	146/−45	375.0	798.1	423.1	832.2	1500	667.8	15
Kangaroo Well, Central Australia	129.7/−29.7	387.8	448.8	61.0	237.1	450	212.9	16
Yunnan Province, SW China	95/22	566.7	2167.4	1600.7	1136.1	1235	98.9	17
Shanwang, China	116.5/38.5	1056.2	1107.0	50.7	725.4	1139	413.1	18
Shanwang, China	116.5/38.5	1056.2	1107.0	50.7	725.4	1494	768.3	19
Picture Gorge Subgroup, North America	−114.7/44.8	808.9	797.1	−11.8	266	700	434	22
Eastern Oregon, North America	−114/45	808.9	837.1	28.2	266	851	585	23
			Mean:	245			509	

[a] Where paleocoordinates are not provided by reference values are calculated using modern coordinates, a plate kinematic model and the rotations of Müller et al. (2008).
[b] Column three subtracted from column four.
[c] Uses the dataset of Willmott and Matsuura (2001) for land precipitation spanning 1950–1999.
[d] Where a range of values is given, the midpoint is used.
[e] Column six subtracted from column seven.
[f] References are as in Table 2.

Alternatively, Ruddiman and Kutzbach (1989) find that relatively high North American topography results in summer drying of the west coast due to onshore winds acquiring a more northerly aspect. This is associated with the western limb of the deepening summer low that forms over North America as mountain ranges are uplifted (Ruddiman and Kutzbach 1989). Northerly winds in summer are observed along the west coast in both cases (Figs. 9a and 9d). The uplift history of North America is controversial, although a recent isotope study suggests high elevations by the Eocene–Oligocene (Mix et al. 2011), which is broadly reflected by the prescribed elevation in our model (75% of the modern; Herold et al. 2008). Thus, if lower elevations are considered then this may partially explain the absence of wet summers along the west coast in our Miocene case. We also note that reproduction of precipitation patterns are significantly improved under the high-resolution configurations of the CCSM3 (cf. Meehl et al. 2006) and improved convection schemes (Boos and Kuang 2010).

c. *Atmospheric changes*

The poleward shift of the subtropical jet streams in the Miocene is consistent with model simulations of increasing CO_2 (Lorenz and DeWeaver 2007). However, the entire shift in our Miocene case occurs during DJF (Fig. 5). The timing and seasonal nature of these changes may be attributable to the sensitivity of the subtropical jet streams to extratropical stratospheric cooling (Fig. 4). Polvani and Kushner (2002) show that cooling of the polar stratosphere causes a poleward shift of the subtropical jet stream, a response which strengthens with increases in lapse rate. Thus as no significant cooling of the Northern Hemisphere polar stratosphere occurs during JJA (cf. Figs. 4c and 4d), no poleward shift of the summer subtropical jet streams is simulated (Fig. 5c). The significant increase in the Northern Hemisphere polar vertical temperature gradient during DJF (Fig. 4d) is also responsible for the stronger zonal wind response of the northern polar jet compared to the Southern Hemisphere (Fig. 5d). This stronger cooling increases relative humidity, which subsequently fuels cloud genesis. However, the cause of this cooling, and why it occurs only in the Northern Hemisphere during winter, is not clear from model diagnostics. Interestingly, uniform bipolar cooling of the stratosphere is modeled in modern doubled CO_2 experiments (Rind et al. 1998) and under Paleocene boundary conditions (Rind et al. 2001), suggesting the unipolar response in our results may be a consequence of Miocene topography.

Miocene eddy kinetic energy maxima also shift poleward during DJF (Fig. 6d). However, only the Northern Hemisphere storm tracks intensify during these months, while the Southern Hemisphere storm tracks weaken. During JJA, both northern and Southern Hemisphere storm tracks weaken in the Miocene (Fig. 6c). Poleward shift of the storm tracks, like zonal circulation, is consistent with the effects of increasing CO_2 (Yin 2005). Similarly, the modeled expansion of the Hadley cells is consistent with an increase in global mean temperature (Frierson et al. 2007).

d. *Experiment caveats*

Biases in the low-resolution CCSM3 have been previously documented and relate chiefly to coarse-resolution, component coupling and parameterization of subgrid-scale processes (Stan et al. 2010; Yeager et al. 2006). Modeling time periods prior to instrument records adds further uncertainty regarding model boundary conditions. Parameter biases may also be more or less severe in paleoclimate simulations (e.g., Lyle 1997).

Uncertainties in our topography and bathymetry exist owing to 1) the low resolution with which the CCSM3 represents the physical Earth; the ramifications of low model resolution on model–data comparisons is problematic, as discussed in Herold et al. (2010). 2) Availability of geological evidence limiting our ability to constrain tectonic events in high temporal and spatial detail. For example, fossil flora and oxygen isotope paleoaltimetry suggests that the southern and central Tibetan Plateau reached near modern elevations by 15 Ma (Spicer et al. 2003) or even 35 Ma (Rowley and Currie 2006); however, relatively little is known of the corresponding lateral and north–south uplift of the plateau (Harris 2006 and references therein). Thus the near-modern elevation of the entire Tibetan Plateau in our topography may represent the upper end of possibilities.

Miocene bathymetry is also subject to large uncertainties in areas such as the North Atlantic and Drake Passage. At present, the Greenland–Scotland Ridge provides a crucial barrier to deep-water outflow from the Greenland–Norwegian Seas. However, given that no deep-water formation occurs in the Greenland–Norwegian Seas in our Miocene case the climatic effect of changes in sill depth are uncertain. The relatively deep Greenland–Scotland Ridge in our Miocene case (Fig. 1) appears to be crucial to the northward flow of warm subtropical water below the mixed layer, and it is unclear what effect the blocking of this water would have on surface climate (Herold et al. 2011b, manuscript submitted to *Paleoceanography*). The depth of the Drake Passage is important in determining the formation of North Atlantic Deep Water. Gradual deepening of the Drake Passage has been shown to initiate North Atlantic Deep Water formation, consequently warming the North Atlantic and cooling the South Atlantic (Sijp and England 2004).

While the timing of the Drake Passage opening is controversial it is generally believed to have been at near modern depths by the Miocene. However, it has been suggested that temporary constriction of the passage prior to the middle Miocene may have weakened the Antarctic Circumpolar Current and contributed to Miocene warming (Lagabrielle et al. 2009).

Miocene vegetation is reconstructed from 29 macrofossil records (Wolfe 1985) with minor amendments (Herold et al. 2010). The exclusion of microfossils precludes grasslands and by association the high pressure cells associated with Hadley circulation (Cosgrove et al. 2002), thus our prescribed vegetation may be associated with a climate warmer than is justified. More complete compilations of fossil flora need to be synthesized into vegetation distributions, which consider the current understanding of Miocene hydrology and ocean and atmosphere circulation. Vegetation models can also be utilized, ideally in concert with fossil flora (e.g., Micheels et al. 2007). Middle Miocene vegetation distributions from a dynamic global vegetation model forced with climate model output present a cooler and more detailed global vegetation compared to this study (Henrot et al. 2010). However, while vegetation models circumvent uncertainties in data extrapolation and assumptions of atmospheric and oceanic circulation, they contain their own model uncertainties and are subject to climate model bias (Shellito and Sloan 2006).

In addition to topography, bathymetry and vegetation small parameter differences exist between our Miocene and control cases (CH_4, N_2O, solar constant, aerosols, and orbital values). Such differences make the attribution of climate changes to specific boundary conditions more problematic. However, based on radiative forcing estimates (e.g., Forster et al. 2007) it is arguable that the reduction in our Miocene case of CH_4 and N_2O concentrations as well as the solar constant would constitute a net Miocene cooling. While aerosol radiative forcing is also lower in our Miocene case relative to the control case, this, along with the negligible change in orbital parameters, is unlikely to result in a net cooling. However, this can only be unequivocally determined by a sensitivity experiment and we also note that the wavelengths of optimum absorption by different atmospheric agents overlap. In addition, our control case should, if anything, be warmer than modern observations given that it has equilibrated to the prescribed 1990 concentrations of greenhouse gases. This is in contrast to observations which represent a transient response to radiative forcing up until the period observed (1950–99, Table 2). The net effect of these model inconsistencies is that the simulated warming between our Miocene and control cases should be considered conservative.

Determining the role CO_2 played in early to middle Miocene warmth and subsequent cooling continues to be a large hindrance to understanding Miocene climate. The use of modern CO_2 in our Miocene case plays a potentially large role in explaining the discrepancies with proxy records (Tables 2 and 3). While marine-based CO_2 proxies still place concentrations at approximately present-day values (Henderiks and Pagani 2008; Tripati et al. 2009) recent upward revisions based on pedogenic carbonates (Retallack 2009) and leaf stomata indices (Kürschner et al. 2008; Retallack 2001) suggest CO_2 was considerably higher. Ice sheet modeling (DeConto et al. 2008; Lunt et al. 2008b) also supports a Miocene CO_2 at least as high as the modern (cf. Pagani et al. 1999). Furthermore, chemistry transport modeling suggests CH_4 concentrations were above present during the Miocene (Beerling et al. 2009), thus Miocene greenhouse forcing was very likely higher than prescribed in our Miocene case. Nevertheless, a slab ocean model forced with output from our Miocene case and a doubled CO_2 concentration of 710 ppmv (Herold et al. 2011a) does not exhibit a sufficient lowering of the meridional temperature gradient to explain our model–data discrepancies, consistent with previous studies (Steppuhn et al. 2007; Tong et al. 2009; You et al. 2009).

6. Conclusions

We present quantitative constraints on the Miocene climate system incorporating reconstructed vegetation, topography, and bathymetry. A decrease in the meridional temperature gradient of 6.5°C and increase in global mean temperature of 1.5°C compared to our control case occurs without an increase in CO_2. Therefore a significant portion of Miocene warmth can be attributed to factors other than greenhouse gases. Nevertheless, similar to previous uncoupled models, our model–data analysis implicates above modern CO_2 or similar-acting mechanisms during the Miocene, consistent with stomatal records (Kürschner et al. 2008). More tropical and polar proxy records are required to reliably constrain the meridional temperature gradient.

Energy budget and heat transport calculations indicate that increased ocean heat transport and reduced albedo were responsible for above modern temperatures at high southern latitudes in the Miocene (Herold et al. 2011b, manuscript submitted to *Paleoceanography*). Conversely, reduced atmosphere and ocean heat transport in the Northern Hemisphere indicates that reduced albedo and topography were responsible for warming at high northern latitudes. This dichotomy indicates that both changes in ocean circulation and land characteristics were responsible for early to middle Miocene warmth.

Changes in atmospheric temperature, wind, and eddy kinetic energy are surprisingly consistent with model predictions of future global warming due to increasing CO_2. However, significant intensification of the polar jet stream is only observed in the Northern Hemisphere. Furthermore, poleward displacement of the subtropical jet streams occurs only during DJF. This polar and seasonal asymmetry is attributed to significantly greater cooling of the polar stratosphere during DJF, particularly in the Northern Hemisphere. Results from this study and Herold et al. (2011b, manuscript submitted to *Paleoceanography*) suggest future work should address sensitivity to various changes in topography and bathymetric constrictions, along with elevated greenhouse gas concentrations.

Acknowledgments. This research was undertaken on the NCI National Facility in Canberra, Australia, which is supported by the Australian Commonwealth Government. In addition, parts of this research were funded by NSF Grants to MH, 0450221-EAR and 0902780-ATM. We thank two anonymous reviewers for their constructive feedback.

REFERENCES

Akgün, F., M. S. Kayseri, and M. S. Akkiraz, 2007: Palaeoclimatic evolution and vegetational changes during the late Oligocene-Miocene period in western and central Anatolia (Turkey). *Palaeogeogr., Palaeoclimatol., Palaeoecol.,* **253,** 56–90.

Barron, E. J., and W. H. Peterson, 1991: The Cenozoic ocean circulation based on ocean general circulation model results. *Palaeogeogr., Palaeoclimatol., Palaeoecol.,* **83,** 1–28.

Beerling, D., R. A. Berner, F. T. Mackenzie, M. B. Harfoot, and J. A. Pyle, 2009: Methane and the CH_4 related greenhouse effect over the past 400 million years. *Amer. J. Sci.,* **309,** 97–113.

Bice, K. L., C. R. Scotese, D. Seidov, and E. J. Barron, 2000: Quantifying the role of geographic change in Cenozoic ocean heat transport using uncoupled atmosphere and ocean models. *Palaeogeogr., Palaeoclimatol., Palaeoecol.,* **161,** 295–310.

Bohme, M., A. A. Bruch, and A. Selmeier, 2007: The reconstruction of early and middle Miocene climate and vegetation in Southern Germany as determined from the fossil wood flora. *Palaeogeogr., Palaeoclimatol., Palaeoecol.,* **253,** 107–130.

Boos, W. R., and Z. Kuang, 2010: Dominant control of the South Asian monsoon by orographic insulation versus plateau heating. *Nature,* **463,** 218–222.

Butzin, M., G. Lohmann, and T. Bickert, 2011: Miocene ocean circulation inferred from marine carbon cycle modeling combined with benthic isotope records. *Paleoceanography,* **26,** PA1203.

Collins, W. D., and Coauthors, 2006: The Community Climate System Model version 3 (CCSM3). *J. Climate,* **19,** 2122–2143.

Cosgrove, B. A., E. J. Barron, and D. Pollard, 2002: A simple interactive vegetation model coupled to the GENESIS GCM. *Global Planet. Change,* **32,** 253–278.

DeConto, R. M., D. Pollard, P. A. Wilson, H. Palike, C. H. Lear, and M. Pagani, 2008: Thresholds for Cenozoic bipolar glaciation. *Nature,* **455,** 652–656.

Dutton, J. F., and E. J. Barron, 1997: Miocene to present vegetation changes: A possible piece of the Cenozoic cooling puzzle. *Geology,* **25,** 39–41.

Eldrett, J. S., I. C. Harding, P. A. Wilson, E. Butler, and A. P. Roberts, 2007: Continental ice in Greenland during the Eocene and Oligocene. *Nature,* **446,** 176–179.

Erdei, B., L. Hably, M. Kazmer, T. Utescher, and A. A. Bruch, 2007: Neogene flora and vegetation development of the Pannonian domain in relation to palaeoclimate and palaeogeography. *Palaeogeogr., Palaeoclimatol., Palaeoecol.,* **253,** 131–156.

Flower, B. P., and J. P. Kennett, 1994: The middle Miocene climatic transition: East Antarctic ice sheet development, deep ocean circulation and global carbon cycling. *Palaeogeogr., Palaeoclimatol., Palaeoecol.,* **108,** 537–555.

——, and ——, 1995: Middle Miocene deepwater paleoceanography in the southwest Pacific: Relations with East Antarctic ice sheet development. *Paleoceanography,* **10,** 1095–1112.

Fluteau, F., G. Ramstein, and J. Besse, 1999: Simulating the evolution of the Asian and African monsoons during the past 30 Myr using an atmospheric general circulation model. *J. Geophys. Res.,* **104,** 11 995–12 018.

Forster, P., and Coauthors, 2007: Changes in atmospheric constituents and in radiative forcing. *Climate Change 2007: The Physical Science Basis,* S. Solomon et al., Eds., Cambridge University Press, 129–234.

Frierson, D. M. W., J. Lu, and G. Chen, 2007: Width of the Hadley cell in simple and comprehensive general circulation models. *Geophys. Res. Lett.,* **34,** L18804, doi:10.1029/2007GL031115.

Greenwood, D. R., 1994: Palaeobotanical evidence for Tertiary climates. *The History of Australian Vegetation: Cretaceous to Recent,* R. S. Hill, Ed., Cambridge University Press, 44–59.

Gregory-Wodzicki, K. M., W. C. McIntosh, and K. Velasquez, 1998: Climatic and tectonic implications of the late Miocene Jakokkota flora, Bolivian Altiplano. *J. South Amer. Earth Sci.,* **11,** 533–560.

Guo, Z. T., and Coauthors, 2008: A major reorganization of Asian climate by the early Miocene. *Climate Past,* **4,** 153–174.

Harris, N., 2006: The elevation history of the Tibetan Plateau and its implications for the Asian monsoon. *Palaeogeogr., Palaeoclimatol., Palaeoecol.,* **241,** 4–15.

Haywood, A. M., and P. J. Valdes, 2004: Modelling Pliocene warmth: Contribution of atmosphere, oceans and cryosphere. *Earth Planet. Sci. Lett.,* **218,** 363–377.

Heinemann, M., J. H. Jungclaus, and J. Marotzke, 2009: Warm Paleocene/Eocene climate as simulated in ECHAM5/MPI-OM. *Climate Past,* **5,** 785–802.

Henderiks, J., and M. Pagani, 2008: Coccolithophore cell size and the Paleogene decline in atmospheric CO2. *Earth Planet. Sci. Lett.,* **269,** 576–584.

Henrot, A. J., L. François, E. Favre, M. Butzin, M. Ouberdous, and G. Munhoven, 2010: Effects of CO2, continental distribution, topography and vegetation changes on the climate at the Middle Miocene: A model study. *Climate Past,* **6,** 675–694.

Herold, N., M. Seton, R. D. Müller, Y. You, and M. Huber, 2008: Middle Miocene tectonic boundary conditions for use in climate models. *Geochem., Geophys., Geosyst.,* **9,** Q10009, doi:10.1029/2008GC002046.

——, R. D. Muller, and M. Seton, 2010: Comparing early to middle Miocene terrestrial climate simulations with geological data. *Geosphere,* **6,** 952–961.

——, M. Huber, D. R. Greenwood, R. D. Müller, and M. Seton, 2011a: Early to Middle Miocene monsoon climate in Australia. *Geology,* **39,** 3–6.

Holbourn, A., W. Kuhnt, M. Schulz, and H. Erlenkeuser, 2005: Impacts of orbital forcing and atmospheric carbon dioxide on Miocene ice-sheet expansion. *Nature,* **438,** 483–487.

Huber, M., and L. C. Sloan, 2001: Heat transport, deep waters, and thermal gradients: Coupled simulation of an Eocene greenhouse climate. *Geophys. Res. Lett.,* **28,** 3481–3484.

Ivanov, D., A. R. Ashraf, V. Mosbrugger, and E. Palamarev, 2002: Palynological evidence for Miocene climate change in the Forecarpathian Basin (Central Paratethys, NW Bulgaria). *Palaeogeogr., Palaeoclimatol., Palaeoecol.,* **178,** 19–37.

Kemp, E. M., 1978: Tertiary climatic evolution and vegetation history in the Southeast Indian Ocean region. *Palaeogeogr., Palaeoclimatol., Palaeoecol.,* **24,** 169–208.

Kiehl, J. T., and C. A. Shields, 2005: Climate simulation of the latest Permian: Implications for mass extinction. *Geology,* **33,** 757–760.

——, ——, J. J. Hack, and W. D. Collins, 2006: The climate sensitivity of the Community Climate System Model version 3 (CCSM3). *J. Climate,* **19,** 2584–2596.

Kürschner, W. M., Z. Kvacek, and D. L. Dilcher, 2008: The impact of Miocene atmospheric carbon dioxide fluctuations on climate and the evolution of terrestrial ecosystems. *Proc. Natl. Acad. Sci. USA,* **105,** 449–453.

Kutzbach, J. E., and P. Behling, 2004: Comparison of simulated changes of climate in Asia for two scenarios: Early Miocene to present, and present to future enhanced greenhouse. *Global Planet. Change,* **41,** 157–165.

Lagabrielle, Y., Y. Goddéris, Y. Donnadieu, J. Malavieille, and M. Suarez, 2009: The tectonic history of Drake Passage and its possible impacts on global climate. *Earth Planet. Sci. Lett.,* **279,** 197–211.

Langebroek, P. M., A. Paul, and M. Schulz, 2009: Antarctic ice-sheet response to atmospheric CO_2 and insolation in the Middle Miocene. *Climate Past,* **5,** 633–646.

Larsen, H. C., 1994: Seven million years of glaciation in Greenland. *Science,* **264,** 952–955.

Lear, C. H., H. Elderfield, and P. A. Wilson, 2000: Cenozoic deep-sea temperatures and global ice volumes from Mg/Ca in benthic foraminiferal calcite. *Science,* **287,** 269–272.

Liang, M.-M., A. Bruch, M. Collinson, V. Mosbrugger, C.-S. Li, Q.-G. Sun, and J. Hilton, 2003: Testing the climatic estimates from different palaeobotanical methods: An example from the Middle Miocene Shanwang flora of China. *Palaeogeogr., Palaeoclimatol., Palaeoecol.,* **198,** 279–301.

Lorenz, D. J., and E. T. DeWeaver, 2007: Tropopause height and zonal wind response to global warming in the IPCC scenario integrations. *J. Geophys. Res.,* **112,** D10119, doi:10.1029/2006JD008087.

Lunt, D. J., R. Flecker, P. J. Valdes, U. Salzmann, R. Gladstone, and A. M. Haywood, 2008a: A methodology for targeting palaeo proxy data acquisition: A case study for the terrestrial late Miocene. *Earth Planet. Sci. Lett.,* **271,** 53–62.

——, G. L. Foster, A. M. Haywood, and E. J. Stone, 2008b: Late Pliocene Greenland glaciation controlled by a decline in atmospheric CO_2 levels. *Nature,* **454,** 1102–1105.

——, P. J. Valdes, A. Haywood, and I. C. Rutt, 2008c: Closure of the Panama Seaway during the Pliocene: Implications for climate and Northern Hemisphere glaciation. *Climate Dyn.,* **30,** 1–18.

Lyle, M., 1997: Could early Cenozoic thermohaline circulation have warmed the poles? *Paleoceanography,* **12,** 161–167.

——, D. Wilkins, J. Barron, and L. Heusser, 2003: North Pacific Sea Surface Temperature, Western U.S. Vegetation, and the Demise of the Miocene Rocky Mountain Monsoon. *Eos, Trans. Amer. Geophys. Union,* 84 (Fall Meeting Suppl.), Abstract PP21C-1185.

——, and Coauthors, 2008: Pacific Ocean and Cenozoic evolution of climate. *Rev. Geophys.,* **46,** RG2002, doi:10.1029/2005RG000190.

Meehl, G. A., J. M. Arblaster, D. M. Lawrence, A. Seth, E. K. Schneider, B. P. Kirtman, and D. Min, 2006: Monsoon regimes in the CCSM3. *J. Climate,* **19,** 2482–2495.

——, and Coauthors, 2007: Global climate projections. *Climate Change 2007: The Physical Science Basis,* S. Solomon et al., Eds., Cambridge University Press, 747–845.

Megirian, D., P. Murray, L. Schwartz, and C. Von Der Borch, 2004: Late Oligocene kangaroo well local fauna from the Ulta Limestone (new name), and climate of the Miocene oscillation across central Australia. *Aust. J. Earth Sci.,* **51,** 701–741.

Micheels, A., A. A. Bruch, D. Uhl, T. Utescher, and V. Mosbrugger, 2007: A late Miocene climate model simulation with ECHAM4/ML and its quantitative validation with terrestrial proxy data. *Palaeogeogr., Palaeoclimatol., Palaeoecol.,* **253,** 251–270.

——, ——, and V. Mosbrugger, 2009a: Miocene climate modelling sensitivity experiments for different CO_2 concentrations. *Palaeontol. Electronica,* **12** (2), 1–20.

——, J. Eronen, and V. Mosbrugger, 2009b: The late Miocene climate response to a modern Sahara desert. *Global Planet. Change,* **67,** 193–204.

——, A. A. Bruch, J. Eronen, M. Fortelius, M. Harzhauser, T. Utescher, and V. Mosbrugger, 2011: Analysis of heat transport mechanisms from a late Miocene model experiment with a fully-coupled atmosphere-ocean general circulation model. *Palaeogeogr., Palaeoclimatol., Palaeoecol.,* **304,** 337–350.

Miller, G., J. Mangan, D. Pollard, S. Thompson, B. Felzer, and J. Magee, 2005: Sensitivity of the Australian Monsoon to insolation and vegetation: Implications for human impact on continental moisture balance. *Geology,* **33,** 65–68.

Miller, K. G., J. D. Wright, and R. G. Fairbanks, 1991: Unlocking the ice house: Oligocene–Miocene oxygen isotopes, eustasy, and margin erosion. *J. Geophys. Res.,* **96,** 6829–6848.

Mix, H. T., A. Mulch, M. L. Kent-Corson, and C. P. Chamberlain, 2011: Cenozoic migration of topography in the North American Cordillera. *Geology,* **39,** 87–90.

Moran, K., and Coauthors, 2006: The Cenozoic palaeoenvironment of the Arctic Ocean. *Nature,* **441,** 601–605.

Mosbrugger, V., and T. Utescher, 1997: The coexistence approach–a method for quantitative reconstructions of tertiary terrestrial palaeoclimate data using plant fossils. *Palaeogeogr., Palaeoclimatol., Palaeoecol.,* **134,** 61–86.

——, ——, and D. L. Dilcher, 2005: Cenozoic continental climatic evolution of Central Europe. *Proc. Natl. Acad. Sci. USA,* **102,** 14 964–14 969.

Müller, R. D., M. Sdrolias, C. Gaina, and W. R. Roest, 2008: Age, spreading rates and spreading asymmetry of the world's ocean crust. *Geochem., Geophys., Geosyst.,* **9,** Q04006, doi:10.1029/2007GC001743.

Otto-Bliesner, B. L., and G. R. Upchurch, 1997: Vegetation-induced warming of high-latitude regions during the Late Cretaceous period. *Nature,* **385,** 804–807.

Pagani, M., M. A. Arthur, and K. H. Freeman, 1999: Miocene evolution of atmospheric carbon dioxide. *Paleoceanography,* **14,** 273–292.

Pearson, P. N., and M. R. Palmer, 2000: Atmospheric carbon dioxide concentrations over the past 60 million years. *Nature,* **406,** 695–699.

Pekar, S. F., and R. M. DeConto, 2006: High-resolution ice-volume estimates for the early Miocene: Evidence for a dynamic ice sheet in Antarctica. *Palaeogeogr., Palaeoclimatol., Palaeoecol.,* **231,** 101–109.

Polvani, L. M., and P. J. Kushner, 2002: Tropospheric response to stratospheric perturbations in a relatively simple general circulation model. *Geophys. Res. Lett.,* **29,** 1114.

Poore, H. R., R. Samworth, N. J. White, S. M. Jones, and I. N. McCave, 2006: Neogene overflow of Northern Component Water at the Greenland-Scotland Ridge. *Geochem., Geophys., Geosyst.,* **7,** Q06010, doi:10.1029/2005GC001085.

Potter, P. E., and P. Szatmari, 2009: Global Miocene tectonics and the modern world. *Earth Sci. Rev.,* **96,** 279–295.

Prell, W. L., and J. E. Kutzbach, 1992: Sensitivity of the Indian monsoon to forcing parameters and implications for its evolution. *Nature,* **360,** 647–652.

Ramsay, A. T. S., C. W. Smart, and J. C. Zachos, 1998: A model of early to middle Miocene deep ocean circulation for the Atlantic and Indian oceans. *Geological evolution of Ocean Basins: Results from the Ocean Drilling Program,* A. Cramp et al., Eds., Geological Society of London, 55-70.

Randel, W. J., F. Wu, H. Vömel, G. E. Nedoluha, and P. Forster, 2006: Decreases in stratospheric water vapor after 2001: Links to changes in the tropical tropopause and the Brewer-Dobson circulation. *J. Geophys. Res.,* **111,** D12312, doi:10.1029/2005JD006744.

Retallack, G. J., 2001: A 300-million-year record of atmospheric carbon dioxide from fossil plant cuticles. *Nature,* **411,** 287–290.

——, 2004: Late Miocene climate and life on land in Oregon within a context of Neogene global change. *Palaeogeogr., Palaeoclimatol., Palaeoecol.,* **214,** 97–123.

——, 2009: Refining a pedogenic-carbonate CO2 paleobarometer to quantify a middle Miocene greenhouse spike. *Palaeogeogr., Palaeoclimatol., Palaeoecol.,* **281,** 57–65.

Rind, D., D. Shindell, P. Lonergan, and N. K. Balachandran, 1998: Climate change and the middle atmosphere. Part III: The doubled CO_2 climate revisited. *J. Climate,* **11,** 876–894.

——, M. Chandler, P. Lonergan, and J. Lerner, 2001: Climate change and the middle atmosphere 5. Paleostratosphere in cold and warm climates. *J. Geophys. Res.,* **106,** 20 195–20 212.

Rögl, F., 1999: Mediterranean and Paratethys. Facts and hypotheses of an Oligocene to Miocene paleogeography: Short overview. *Geol. Carpathica,* **50,** 339–349.

Rosenfield, J. E., 1993: Radiative feedback of polar stratospheric clouds on Antarctic temperatures. *Geophys. Res. Lett.,* **20,** 1195–1198.

Rowley, D. B., and B. S. Currie, 2006: Palaeo-altimetry of the late Eocene to Miocene Lunpola basin, central Tibet. *Nature,* **439,** 677–681.

Ruddiman, W. F., and J. E. Kutzbach, 1989: Forcing of late Cenozoic Northern Hemisphere climate by plateau uplift in southern Asia and the American west. *J. Geophys. Res.,* **94,** 18 409–18 427.

——, ——, and I. C. Prentice, 1997: Testing the climatic effects of orography and CO2 with general circulation and biome models. *Tectonic Uplift and Climate Change,* W. F. Ruddiman, Ed., Plenum Press, 203–235.

Schnitker, D., 1980: North Atlantic oceanography as possible cause of Antarctic glaciation and eutrophication. *Nature,* **284,** 615–616.

Sheldon, N. D., 2006: Using paleosols of the Picture Gorge Basalt to reconstruct the middle Miocene climatic optimum. *PaleoBios,* **26,** 27–36.

Shellito, C. J., and L. C. Sloan, 2006: Reconstructing a lost Eocene paradise. Part II: On the utility of dynamic global vegetation models in pre-Quaternary climate studies. *Global Planet. Change,* **50,** 18–32.

——, J.-F. Lamarque, and L. C. Sloan, 2009: Early Eocene Arctic climate sensitivity to pCO_2 and basin geography. *Geophys. Res. Lett.,* **36,** L09707, doi:10.1029/2009GL037248.

Shevenell, A. E., J. P. Kennett, and D. W. Lea, 2008: Middle Miocene ice sheet dynamics, deep-sea temperatures, and carbon cycling: A Southern Ocean perspective. *Geochem., Geophys., Geosyst.,* **9,** Q02006, doi:10.1029/2007GC001736.

Sijp, W. P., and M. H. England, 2004: Effect of the Drake Passage Throughflow on global climate. *J. Phys. Oceanogr.,* **34,** 1254–1266.

Sloan, L. C., and D. Pollard, 1998: Polar stratospheric clouds: A high latitude warming mechanism in an ancient greenhouse world. *Geophys. Res. Lett.,* **25,** 3517–3520.

——, J. C. G. Walker, and T. C. Moore, Jr., 1995: Possible role of oceanic heat transport in early Eocene climate. *Paleoceanography,* **10,** 347–356.

Sluiter, I. R. K., A. P. Kershaw, G. R. Holdgate, and D. Bulman, 1995: Biogeographic, ecological and stratigraphic relationships of the Miocene brown coal floras, Latrobe Valley, Victoria, Australia. *Int. J. Coal Geol.,* **28,** 277–302.

Spicer, R. A., and Coauthors, 2003: Constant elevation of southern Tibet over the past 15 million years. *Nature,* **421,** 622–624.

Stan, C., and Coauthors, 2010: An ocean–atmosphere climate simulation with an embedded cloud resolving model. *Geophys. Res. Lett.,* **37,** L01702, doi:10.1029/2009GL040822.

Steppuhn, A., A. Micheels, G. Geiger, and V. Mosbrugger, 2006: Reconstructing the Late Miocene climate and oceanic heat flux using the AGCM ECHAM4 coupled to a mixed-layer ocean model with adjusted flux correction. *Palaeogeogr., Palaeoclimatol., Palaeoecol.,* **238,** 399–423.

——, ——, A. Bruch, D. Uhl, T. Utescher, and V. Mosbrugger, 2007: The sensitivity of ECHAM4/ML to a double CO_2 scenario for the Late Miocene and the comparison to terrestrial proxy data. *Global Planet. Change,* **57,** 189–212.

Sun, Q.-G., M. E. Collinson, C.-S. Li, Y.-F. Wang, and D. J. Beerling, 2002: Quantitative reconstruction of palaeoclimate from the Middle Miocene Shanwang flora, eastern China. *Palaeogeogr., Palaeoclimatol., Palaeoecol.,* **180,** 315–329.

Syabryaj, S., T. Utescher, S. Molchanoff, and A. A. Bruch, 2007: Vegetation and palaeoclimate in the Miocene of Ukraine. *Palaeogeogr., Palaeoclimatol., Palaeoecol.,* **253,** 169–184.

Tong, J. A., Y. You, R. D. Müller, and M. Seton, 2009: Climate model sensitivity to atmospheric CO_2 concentrations for the middle Miocene. *Global Planet. Change,* **67,** 129–140.

Tripati, A. K., C. D. Roberts, and R. A. Eagle, 2009: Coupling of CO_2 and ice sheet stability over major climate transitions of the last 20 million years. *Science,* **326,** 1394–1397.

Uhl, D., V. Mosbrugger, A. Bruch, and T. Utescher, 2003: Reconstructing palaeotemperatures using leaf floras—Case studies for a comparison of leaf margin analysis and the coexistence approach. *Rev. Palaeobot. Palynol.,* **126,** 49–64.

——, A. A. Bruch, C. Traiser, and S. Klotz, 2006: Palaeoclimate estimates for the Middle Miocene Schrotzburg flora (S Germany): A multi-method approach. *Int. J. Earth Sci.,* **95,** 1071–1085.

——, S. Klotz, C. Traiser, C. Thiel, T. Utescher, E. Kowalski, and D. L. Dilcher, 2007: Cenozoic paleotemperatures and leaf physiognomy—A European perspective. *Palaeogeogr., Palaeoclimatol., Palaeoecol.,* **248,** 24–31.

Utescher, T., V. Mosbrugger, and A. R. Ashraf, 2000: Terrestrial climate evolution in northwest Germany over the last 25 million years. *Palaios,* **15,** 430–449.

——, D. Djordjevic-Milutinovic, A. Bruch, and V. Mosbrugger, 2007: Palaeoclimate and vegetation change in Serbia during the last 30 Ma. *Palaeogeogr., Palaeoclimatol., Palaeoecol.,* **253,** 157–168.

von der Heydt, A., and H. A. Dijkstra, 2006: Effect of ocean gateways on the global ocean circulation in the late Oligocene and early Miocene. *Paleoceanography,* **21,** PA1011, doi:10.1029/2005PA001149.

Wang, C., and Coauthors, 2008: Constraints on the early uplift history of the Tibetan Plateau. *Proc. Natl. Acad. Sci. USA,* **105,** 4987–4992.

White, J. M., and T. A. Ager, 1994: Palynology, paleoclimatology and correlation of Middle Miocene beds from Porcupine River (locality 90-1), Alaska. *Quat. Int.,* **22–23,** 43–77.

Wiemann, M. C., S. R. Manchester, and E. A. Wheeler, 1999: Paleotemperature estimation from dicotyledonous wood anatomical characters. *Palaios,* **14,** 459–474.

Willmott, C. J., and K. Matsuura, cited 2001: Terrestrial air temperature and precipitation: Monthly and annual time series (1950–1999). [Available online at http://climate.geog.udel.edu/~climate.]

Wolfe, J. A., 1985: Distribution of major vegetational types during the Tertiary. *The Carbon Cycle and Atmopsheric CO2, Geophys. Monogr.,* Vol. 32, American Geophysical Union, 357–375.

——, 1994a: Tertiary climatic changes at middle latitudes of western North America. *Palaeogeogr., Palaeoclimatol., Palaeoecol.,* **108,** 195–205.

——, 1994b: An analysis of Neogene climates in Beringia. *Palaeogeogr., Palaeoclimatol., Palaeoecol.,* **108,** 207–216.

Woodruff, F., and S. M. Savin, 1989: Miocene deepwater oceanography. *Paleoceanography,* **4,** 87–140.

Wright, J. D., and K. G. Miller, 1996: Control of North Atlantic Deep Water circulation by the Greenland–Scotland Ridge. *Paleoceanography,* **11,** 157–170.

Yang, J., Y.-F. Wang, R. A. Spicer, V. Mosbrugger, C.-S. Li, and Q.-G. Sun, 2007: Climatic reconstruction at the Miocene Shanwang basin, China, using leaf margin analysis, CLAMP, coexistence approach, and overlapping distribution analysis. *Amer. J. Bot.*, **94,** 599–608.

Yeager, S. G., C. A. Shields, W. G. Large, and J. J. Hack, 2006: The low-resolution CCSM3. *J. Climate,* **19,** 2545–2566.

Yin, J. H., 2005: A consistent poleward shift of the storm tracks in simulations of 21st century climate. *Geophys. Res. Lett.,* **32,** L18701, doi:10.1029/2005GL023684.

You, Y., M. Huber, R. D. Müller, C. J. Poulsen, and J. Ribbe, 2009: Simulation of the middle Miocene climate optimum. *Geophys. Res. Lett.,* **36,** L04702, doi:10.1029/2008GL036571.

Zachos, J. C., M. Pagani, L. Sloan, E. Thomas, and K. Billups, 2001: Trends, rhythms, and aberrations in global climate 65 Ma to present. *Science,* **292,** 686–693.

——, G. R. Dickens, and R. E. Zeebe, 2008: An early Cenozoic perspective on greenhouse warming and carbon-cycle dynamics. *Nature,* **451,** 279–283.

Zhao, L.-C., Y.-F. Wang, C.-J. Liu, and C.-S. Li, 2004: Climatic implications of fruit and seed assemblage from Miocene of Yunnan, southwestern China. *Quat. Int.,* **117,** 81–89.

Zhongshi, Z., W. Huijun, G. Zhengtang, and J. Dabang, 2007a: Impacts of tectonic changes on the reorganization of the Cenozoic paleoclimatic patterns in China. *Earth Planet. Sci. Lett.,* **257,** 622–634.

——, H. Wang, Z. Guo, and D. Jiang, 2007b: What triggers the transition of palaeoenvironmental patterns in China, the Tibetan Plateau uplift or the Paratethys Sea retreat? *Palaeogeogr., Palaeoclimatol., Palaeoecol.,* **245,** 317–331.